Research on Chemical Intermediates
https://doi.org/10.1007/s11164-024-05309-2

Non-oxidative ethane dehydrogenation reaction over molybdenum and chromium incorporated MgO encapsulated carbon-core catalysts in microwave reactor

Birce Pekmezci Karaman[1] · **Emine Kaya Ekinci**[1]

Received: 19 February 2024 / Accepted: 6 May 2024
© The Author(s) 2024

Abstract
Chromium and molybdenum incorporated MgO and MgO–C catalysts were synthesized for hydrogen production from a non-oxidative ethane dehydration reaction. Hydrogen production studies were carried out using a microwave-heated reactor system. The study investigated the effects of reaction temperature, type of active metal, and catalyst preparation method (physical mixture or core–shell structure) on hydrogen selectivity and ethane conversion during dehydrogenation reactions. The results showed that the optimal reaction temperature for the non-oxidative ethane dehydration reaction was 450 °C. Above this temperature, the selectivity of undesired byproducts increased. Catalysts containing molybdenum exhibited higher ethane conversion. Moreover, a comparison of MgO–C-supported catalysts with MgO-supported catalysts revealed that the core–shell catalysts exhibited superior ethane conversion. Notably, the 5Mo@MgO–C catalyst demonstrated exceptional catalytic activity, achieving a high ethane conversion rate of 72% along with excellent stability.

Keywords Magnesium oxide · Mesoporous carbon · Core–shell catalysts · Ethane · Hydrogen · Dehydrogenation · Microwave reactor

Introduction

Fossil fuels such as coal, natural gas, and oil continue to be our primary energy sources today. However, the growing global population and technological advancements have resulted in the rapid depletion of fossil fuels. Fossil fuels are

✉ Emine Kaya Ekinci
eminekaya@gazi.edu.tr

Birce Pekmezci Karaman
bircepekmezci@gazi.edu.tr

[1] Department of Chemical Engineering, Gazi University, 06570 Ankara, Turkey

Published online: 21 May 2024

primarily used as automotive fuels and there are approximately 1.25 billion vehicles on the planet today. With the advancement of technology, the number of vehicles is expected to reach about 2 billion by 2050. Common pollutants produced by vehicles that burn fossil fuels include carbon dioxide (CO2), carbon monoxide (CO), nitrogen oxides (NOx), methane (CH4), and sulfur dioxide (SO2) [1]. Clean, environmentally friendly, inexhaustible, and renewable energy sources are required for these vehicles, and among such energy sources, hydrogen energy has gained importance with the development of fuel cell technology [2, 3].

Hydrogen, which is a clean fuel, produces only water when consumed in a fuel cell. However, pure hydrogen gas is scarce in nature. Hydrocarbon compounds contain significant amounts of hydrogen. There are numerous studies on hydrogen production in the literature, and it is known that the thermal processing of biomass sources yields a substantial amount of hydrogen. Examples include the steam-reforming reaction of acetic acid [4], the dry-reforming reaction of methane [5], and biomass gasification/pyrolysis processes [6]. However, in these processes, in addition to hydrogen production, byproducts are also formed. The occurrence of reformation and gasification/pyrolysis reactions leads to the generation of CO_2 and CO gases, coexisting with gases that exhibit a notable hydrocarbon content, notably methane. Hydrogen must be free of greenhouse gases in order to be used as a fuel in fuel cells. For example, Pt-based catalysts used in polymer electrolyte membrane (PEM) fuel cells are known to be poisoned in the presence of CO. As a result, CO concentrations should be kept below ten ppm to avoid poisoning the catalyst in PEM fuel cells [7].

In recent years, research has been conducted with the aim of obtaining pure hydrogen through the decomposition of hydrocarbons in an oxygen-free environment, where the produced hydrogen does not contain greenhouse gases. The decomposition of ethane in natural gas in an oxygen-free environment yields hydrogen with high selectivity. As a result of the dehydrogenation reaction of ethane, besides hydrogen, ethylene is obtained (Eq. 1). Ethylene is a raw material used in the manufacture of polyethylene, polyester, polystyrene, polyvinyl chloride, and many other products [2].

$$C_2H_6 \leftrightarrow C_2H_4 + H_2 \quad \Delta H^\circ = 136.4\,\mathrm{kJ\,mol^{-1}} \tag{1}$$

Non-oxidative catalytic ethane dehydrogenation reaction is an endothermic equilibrium reaction. Therefore, high reactant conversion and product selectivity are observed at high reaction temperatures and low reaction pressure. Hydrogen production studies with ethane dehydrogenation reaction were carried out at a reaction temperature of 750–850 °C [8]. High reaction temperature causes the sintering of active metals in catalyst content. In this case, side reactions and undesirable products are observed. Furthermore, a large amount of energy is required to operate at high reaction temperatures. The high energy demand in ethane dehydration is a major concern. As a result, most studies focus on employing the exothermic oxidative ethane dehydrogenation process (Eq. 2). Nevertheless, non-oxidative ethane dehydrogenation possesses a significant advantage over the oxidative reaction due to the production of hydrogen during the reaction.

$$C_2H_6 + {}^1\!/_2\, O_2 \leftrightarrow C_2H_4 + H_2O \;\; \Delta H^\circ = -105.5\,\mathrm{kJ\,mol^{-1}} \tag{2}$$

Depending on the reaction temperature and catalyst selection, certain side reactions may occur, resulting in a decrease in hydrogen selectivity. Methane, acetylene, and coke are significant side products. The decomposition of ethane (Eqs. 3 and 4) and ethylene (Eq. 5) reactions canlead to the formation of methane. Carbon deposition may occur through ethane decomposition (Eqs. 3 and 6), ethylene decomposition (Eq. 5), and methane decomposition (Eq. 7). Acetylene was also obtained with ethane decomposition (Eq. 8).

$$C_2H_6 \leftrightarrow CH_4 + H_2 + C \;\; \Delta H^\circ 298 = 9.3\,\mathrm{kJ/mol} \tag{3}$$

$$C_2H_6 \leftrightarrow CH_4 + 1/2C_2H_4 \;\; \Delta H^\circ 298 = 35.6\,\mathrm{kJ/mol} \tag{4}$$

$$C_2H_4 \leftrightarrow CH_4 + C \;\; \Delta H^\circ 298 = -127\,\mathrm{kJ/mol} \tag{5}$$

$$C_2H_6 \leftrightarrow 3H_2 + 2C \;\; \Delta H^\circ 298 = 83.8\,\mathrm{kJ/mol} \tag{6}$$

$$CH_4 \leftrightarrow C + 2H_2 \;\; \Delta H^\circ 298 = 74.5\,\mathrm{kJ/mol} \tag{7}$$

$$C_2H_4 \leftrightarrow C_2H_2 + H_2 \;\; \Delta H^\circ 298 = 175\,\mathrm{kJ/mol} \tag{8}$$

Many studies in the literature have concentrated on minimizing by-product formation and mitigating the elevated reaction temperatures induced by the endothermic nature of the reaction, consequently addressing the associated high energy demands. Recently, microwave-heated reaction systems have been preferred for hydrogen production with lower energy consumption and more economical conditions. Heat is transmitted to the catalyst from the walls and cavities of the tube furnace in conventional heated reactor systems. During the reaction, each zone of the tube furnace is heated [9–12]. Heat is produced directly in the catalyst bed in reactor systems that use microwave energy for heating. Since microwave-heated systems only heat the catalyst bed, less energy is consumed to heat the walls and cavities of the reactor system. Thus, more efficient hydrogen production is achieved with lower energy consumption. Microwave-heated reactor systems have numerous advantages over conventionally heated systems, including the following:

- Heat is provided by electromagnetic waves.
- In contrast to conventional heating systems, microwave-assisted heating selectively heats only the catalyst bed, excluding the cavities and walls of the tube furnace.
- By transferring microwave energy directly to the catalyst, heat is generated through the material. Thus, the desired temperature can be reached in a short time.
- Since the catalyst bed is directly heated, temperature differences do not occur inside the reactor. As a result, side effects are reduced [13–17].

Due to these features, microwave-heated systems are advantageous compared to conventional heated reactor systems. Eryıldırım et al. investigated the activity of 5Cr@SBA-15 and carbon fiber catalysts in both conventional and microwave heating reactor systems. Higher ethane conversions at lower temperatures were achieved in the microwave heating system. While 85.7% ethane conversion was achieved at 750 ℃ in the conventional system using 5Cr@SBA-15, the same conversion was reached at 500 ℃ in the microwave system. From 550 ℃ onwards, similar ethane conversion values for both 5Cr@SBA-15 and carbon nanofiber indicate that thermal decomposition becomes dominant. In the conventional system, heat is transferred to the catalyst via conduction and convection mechanisms, potentially leading to a catalyst bed temperature lower than the wall and gap temperatures. In contrast, the microwave system generates heat directly within the catalyst. This direct heating prevents energy losses associated with heating oven walls and gaps, resulting in higher efficiency. Additionally, hot spots, known as microplasmas, form during microwave heating [8]. Seyfeli et al. studied the ammonia decomposition reaction to produce hydrogen without COx using both microwave and conventional heating reactor systems with nickel-based catalysts. They found that the temperature in the microwave system's microplasmas was likely higher than readings from the infrared pyrometer. This was supported by studies where active carbon was used in both types of reactor systems. As a result, between 400 and 550 °C, the Ni@Alumina and Ni@AC catalysts showed significantly lower activity under conventional heating compared to microwave heating at the same temperatures. Previous literature consistently shows that higher temperatures lead to lower activity in conventional heating compared to microwave heating [13]. Therefore, our research group focused on ethane dehydrogenation reaction exclusively in the microwave heating system.

Catalysts in microwave-heated reaction systems must be able to absorb microwave energy. In microwave-heated systems, catalysts are mixed with carbon-containing materials with high dielectric coefficients [18, 19]. Recently, researchers have investigated the activities of catalysts based on chromium (Cr) [20], molybdenum (Mo) [21], nickel (Ni) [22], iron (Fe) [23], and palladium (Pd)[24] for the dehydrogenation of ethane. A review of the literature revealed a particular emphasis on the utilization of supported chromium oxide catalysts, which have demonstrated notable efficacy in dehydrogenation reactions. Molybdenum, distinguished by its unique catalytic properties, plays a crucial role in facilitating the desired transformation of ethane into ethylene by enhancing catalytic activity. As a transition metal, molybdenum exhibits high melting and boiling points. Its catalytic properties render it a frequently employed element in industrial processes, mainly as an effective catalyst in hydrogenation and oxidation reactions. Furthermore, its distinctive characteristics, including enhanced activity and selectivity, coupled with high thermal stability, position molybdenum as a pivotal and valuable catalyst for optimizing the conversion process.

In contrast to the limited studies on the mechanism of non-oxidative dehydrogenation of ethane in the presence of molybdenum catalysts, recent research has shed light on the dehydrogenation mechanism in the presence of chromium (Fig. 1) [25]. This mechanism, as elucidated by Lillehaug et al., [26] revolves around a mononuclear Cr^{3+}-O site supported on a high-surface oxide. The process initiates with

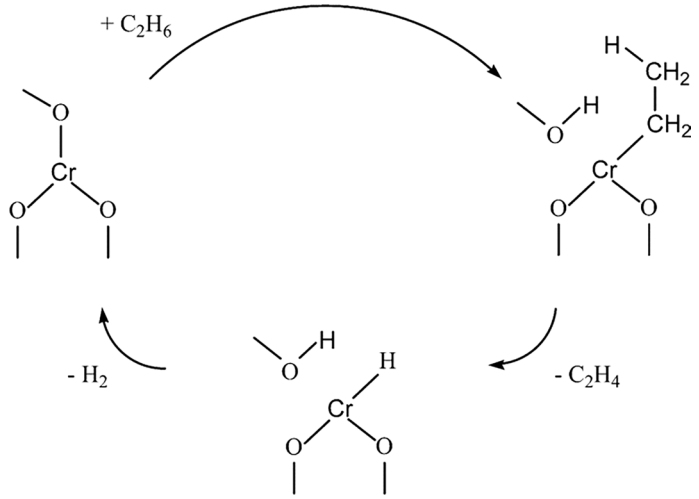


Fig. 1 Schematic reaction mechanism for the dehydrogenation of alkanes over a $Cr.^{3+}$–O active site [25]

ethane reacting with a coordinatively unsaturated Cr^{3+} center, resulting in the formation of a new O–H group and a Cr-alkyl bond. Subsequently, hydrogen transfer from the alkyl to Cr facilitates alkene formation, identified as the rate-determining step. The reaction cycle concludes with the generation of H_2 and the restoration of the Cr^{3+}O active site. Furthermore, an alternative mechanism involves ethane addition to hydrido-chromium sites, leading to the formation of Cr-Ethyl and molecular H_2. The cycle completes with β-H transfer to Cr and ethene desorption [25].

Previous studies have demonstrated that introducing chromium (Cr) and molybdenum (Mo) into MgO leads to a substantial increase in ethane conversion. Moreover, the properties of the support materials have been found to exert significant effects on catalyst activity, product selectivity, and resistance to coke formation. Magnesium oxide (MgO)-supported catalysts containing Cr and Mo were prepared for use in this study. Moreover, mesoporous MgO was used as a support material in the present study due to its redox characteristics, acid-base properties, and crystal structure. As a result of such benefits, mesoporous MgO materials have attracted considerable attention in alternative energy research. MgO catalyst supports were applied in catalytic processes such as the steam reforming of acetic acid [4, 27], dry reforming of methane [28], aqueous phase reforming of glycerol [29], and steam reforming of ethanol [5] to obtain catalysts with better activity and stability. Although MgO can absorb some microwave energy, it cannot be heated sufficiently to achieve the desired reaction conditions. For this reason, it is mixed with mesoporous carbon in experimental studies. However, in physically mixed catalysts, homogeneous mixing cannot be achieved due to the density differences of the materials [30]. As a result, materials are not present in the catalyst bed at the desired ratios, the catalyst cannot be heated uniformly, and reproducible activity may not be observed in reactions performed with physically mixed catalysts. Byproduct formation cannot be avoided in such cases. As an alternative to physically mixed catalysts, "core–shell" materials

have recently begun to be synthesized. Core–shell catalysts are structures formed by coating a core material with another material as a shell. The chemical and thermal stability of compound materials can be increased by coating the shell material onto the core material and new-generation materials can be created [30–32].

Within the scope of this study, both physically mixed catalysts (MgO and mesoporous carbon, 1/1 by mass) and catalysts with a core–shell structure (MgO–C) have been synthesized. Activity tests for the prepared catalysts were conducted using the ethane dehydrogenation reaction in a microwave-heated reactor system. The advantages of microwave heating over conventional methods have been emphasized, highlighting reduced energy consumption and increased efficiency. Additionally, the effects of the catalyst synthesis method on ethane conversion and hydrogen selectivity have been investigated in detail. A novel approach has been introduced by exploring innovative catalysts, such as mesoporous MgO and core–shell structures, while insights into ethane dehydrogenation with chromium and molybdenum catalysts have been provided. In the literature, catalysts often consist of physically mixed components, whereas in this study, a dual-functional catalyst with a core–shell structure has been prepared. The catalysts used in this study have been specifically tailored for ethane dehydrogenation reactions, demonstrating an original contribution to alternative fuel production. Overall, a comprehensive approach to alternative energy research has been offered by integrating microwave heating technology and catalyst innovation in this study.

Experimental

Synthesis of Mo- and Cr-impregnated MgO and MgO–C catalysts

Mesoporous MgO catalyst supports were prepared using a hydrothermal synthesis method based on the work done by Ibrahim et al. [4]. For synthesis, magnesium nitrate hexahydrate ($Mg(NO_3)_2{\cdot}6H_2O$, Sigma Aldrich) was used as a magnesium source, sodium carbonate (Na_2CO_3, Sigma Aldrich) was used as a precipitant agent, and deionized water was used as a solvent. Initially, the prepared solutions were transferred to an autoclave at room temperature, where precipitation occurred. The autoclave was then placed in an oven and heated to 180 °C for a hydrothermal process of 24 h. The autoclave was then cooled to room temperature. The white solid product was filtered, washed with distilled water and absolute ethanol, and dried in an oven at 80 °C. Calcination of the white solid product under a flow of dry air at 800 °C at a heating rate of 5 °C/min for 2 h yielded the MgO catalyst supports.

Core–shell materials (MgO–C) are formed by covering core materials with different shell materials. In the present study, mesoporous MgO with a large surface area and high thermal resistance was coated onto mesoporous carbon to be used as a microwave receptor. Catalysts in the core–shell structure were prepared by the hydrothermal synthesis method. The synthesis method was the same as that applied to the mesoporous MgO catalyst. However, for the preparation of the MgO–C catalyst, the mesoporous carbon catalyst was added to the synthesis solution before hydrothermal synthesis in such a way that the MgO/C ratio was 1/1 by mass.

Active metal-containing catalysts were prepared by loading chrome ($Cr(NO_3)_3$ $9H_2O$, Sigma Aldrich) and molybdenum ($Mo((NH_4)6Mo_7O_{24}$ $4H_2O$, Sigma Aldrich) onto MgO and MgO–C support materials (5% by mass) by wet-impregnation method. Before the impregnation step, the MgO supported catalyst was stirred continuously in deionized water. Mo or Cr was dissolved in deionized water in a separate vessel, and this solution was added drop by drop into the slurry containing the support catalyst. The mixture was then stirred at 40 °C for 24 h for the evaporation of water. The solid product was dried and calcined in dry air. All the calcined catalysts were then reduced under hydrogen flow before the activity tests. Active metal-containing catalysts were prepared by loading Cr and Mo (5% by mass) onto MgO and MgO–C, hereafter called 5Cr@MgO, 5Mo@MgO, 5Cr@MgO–C, and 5Mo@MgO–C.

Catalyst characterization

The synthesized catalysts were subjected to pre-reaction and post-reaction characterization techniques to determine their physical and chemical properties. The catalysts were characterized by techniques including X-ray powder diffraction (XRD), scanning electron microscopy (SEM), transmission electron microscopy (TEM), N_2 adsorption-desorption, and inductively coupled plasma mass spectrometry (ICP-MS). A CuK_α X-ray source equipped with a Rigaku D/MAX 2200 diffractometer was used to obtain low and wide XRD patterns at a rate of 2°/min. A Quanta 400F field-emission high-resolution scanning electron microscope was used to obtain the SEM images of the prepared catalysts. To determine the structure and topography of the MgO–C catalyst, TEM analysis was performed with a high-resolution JEOL JEM-2100F 200 kV HRTEM. Using a Quanta Chrome Autosorp 6 physical adsorption instrument, the specific surface areas, diameters, and volumes of the pores of the synthesized catalysts were determined with the Brunauer–Emmett–Teller (BET) method. The catalyst pores were cleaned out by degassing each material for 2 hours at 120 °C with high vacuum prior to analysis. Following that, N2 adsorption-desorption isotherms were evaluated. ICP-MS analysis was performed using a PerkinElmer DRC II ICP-MS device to determine whether the metal ratios used in the synthesis were compatible with those obtained after synthesis. After the activity tests, thermogravimetric/derivative thermogravimetry (TG/DTG) analysis was also performed for the spent catalysts. Before the activity test studies, Thermogravimetric Analysis (TGA) was conducted to determine the mass loss attributed to the carbon in the core–shell catalyst structure. Subsequently, a TGA analysis of the catalyst was performed after the reaction for spent catalysts. The difference between the two measurements directly corresponds to the carbon formed during the side reactions.

Catalytic performance of the synthesized catalysts

The non-oxidative dehydrogenation of ethane was investigated in a microwave-heated reactor system. In this system, the catalysts were mixed with mesoporous carbon at a ratio of 1:1 (0.05 g of catalyst and 0.05 g mesoporous carbon (Sigma Aldrich)) to

enhance the microwave absorption capacity of the catalyst. The microwave-heated reactor had a maximum operating power of 2 kW and was supplied by SAIREM Company. Microwave power regulation was achieved using a generator and focused directly on the catalyst bed. The generator indicates the set power, the power sent to the catalyst (forward point), and the power not absorbed by the catalyst and reflected (reflected point). The desired reaction temperature was achieved by adjusting the power regulation via precise microwave tuners. To reach a reaction temperature of 450 °C, the power from the microwave generator was set to 0.04 kW. The power sent to the catalyst bed was 0.02 kW, of which 0.01 kW was absorbed by the catalysts and mesoporous carbon mixture. The power reflected without absorption was absorbed by the cooling water sent to the microwave reactor. The temperature was measured using an infrared pyrometer (Raytek M13). The reactor system utilized high-purity ethane (99.5%, from Air Products), which was diluted with argon. Flow control was achieved using mass flowmeters. The feed stream composition was C_2H_6/Ar (99.5%, from Linde) with a molar ratio of 1/2 (GHSV: 18,000 mL/h.gcat). Analysis of the reactants and products was conducted using a gas chromatograph (GC, Agilent Model 6890N) connected to the reactor exit. The GC device was equipped with a Porapak-S column and a thermal conductivity detector. A total carbon balance (Eq. 9). was used to determine the inlet flow rate of ethane. The catalytic activity of the system was evaluated based on ethane conversion (X_{C2H6}), product selectivity (S_i), and yield values, which were calculated using Eqs. 10–12, respectively. Here, F_{C2H6} represents the molar flow rate of either the inlet or outlet flow of the reactor. Moreover, F_i denotes the molar flow rate of hydrogen, ethylene, methane, and acetylene. In addition, turnover number (Eq. 13) and turnover frequency (Eq. 14) were calculated to provide a detailed explanation of the catalysts' activity test results.

$$F_{C_2H_6\,inlet} = F_{C_2H_6\,outlet} + F_{C_2H_4} + {}^1\!/_2\, F_{CH_4} + F_{C_2H_2} \tag{9}$$

$$\mathrm{X}_{\mathrm{C_2H_6}} = \frac{\left(F_{C_2H_6\,inlet} - F_{C_2H_6\,outlet}\right)}{\left(F_{C_2H_6\,inlet}\right)} \tag{10}$$

$$\text{Selectivity}\ \left(S_i\right) = \frac{\left(F_i\right)}{\left(F_{C_2H_6\,inlet} - F_{C_2H_6\,outlet}\right)},\ \text{i:}H_2,\ C_2H_4,\ CH_4,\ C_2H_2 \tag{11}$$

$$\text{Yield}\ \left(Y_i\right) = \frac{\left(F_i\right)}{\left(F_{C_2H_6\,inlet}\right)} \tag{12}$$

$$\mathrm{TON} = \frac{Number\ of\ moles\ of\ reactants\ consumed\ during\ the\ reaction}{\mathrm{Mole\ of\ Catalyst}} \tag{13}$$

$$\mathrm{TOF} = \frac{TON}{\mathrm{Reactiontime}}, min^{-1} \tag{14}$$

Results and discussion

Characterization results of the synthesized catalysts

The synthesized catalysts were analyzed using XRD analysis. The XRD patterns of the catalysts supported on MgO are presented in Fig. 2. The distinct peaks at 2θ angles of 10° and 90°, correspond to cubic MgO material (JCPDS 45-0946). The strong peaks observed at 2θ values of 36.9°, 41.9°, 62.2°, 74.6°, and 78.6° in the MgO material were specifically identified as characteristic of magnesia [29, 33]. The diffraction peaks at 2θ values of 33.77°, 36.26°, 41.44°, and 63.50° in the wide-angle XRD patterns of the reduced catalysts were assigned to Cr2O3 (eskolaite). The main characteristic peak of Cr2O3 at 41.44° overlapped with the diffraction peak of MgO (41.9°) in the XRD pattern of 5Cr@MgO. Moreover, the molybdenum peak that appeared at the 2θ value of 40.50° also overlapped with the diffraction peak of MgO [34].

The XRD results for the core–shell-type MgO–C catalyst are shown in Fig. 3. The characteristic peaks of MgO were identified at 2θ angles of 36.9°, 41.9°, 62.2°, 74.6°, and 78.6°. Furthermore, the peak at 26° indicated the presence of a mesoporous carbon structure in the core–shell-type catalyst. This result demonstrated the successful synthesis of MgO-encapsulated carbon-core catalysts [33]. The wide-angle XRD pattern of the catalysts incorporating active metals indicated the presence of metallic Mo and Cr2O3 in the structure of 5Mo@MgO–C and 5Cr@MgO–C, respectively [8, 35].

The N2 adsorption/desorption isotherms of the support material and the reduced catalysts are presented in Fig. 4. In accordance with the IUPAC classification, the N2 adsorption-desorption isotherms of the catalysts were classified as type IV, indicating their mesoporous structure [35–39]. With the addition of active metals to the structure of the MgO and MgO–C catalysts, the hysteresis loop shifted to higher

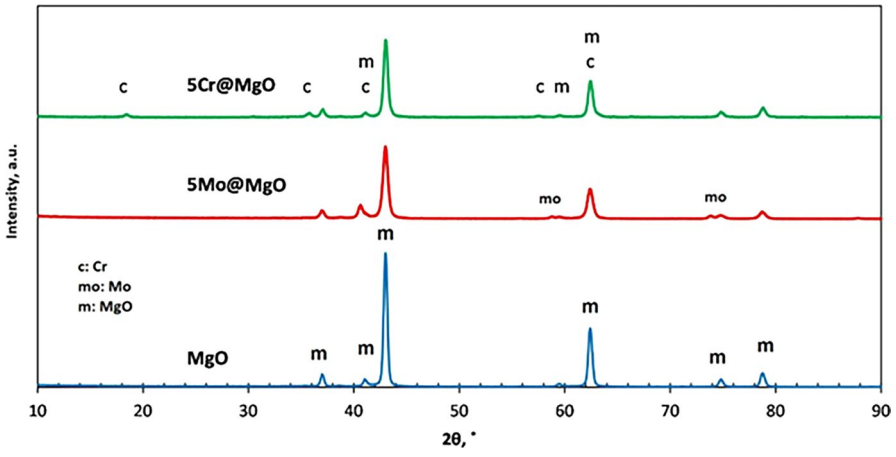


Fig. 2 XRD patterns of MgO-supported catalysts

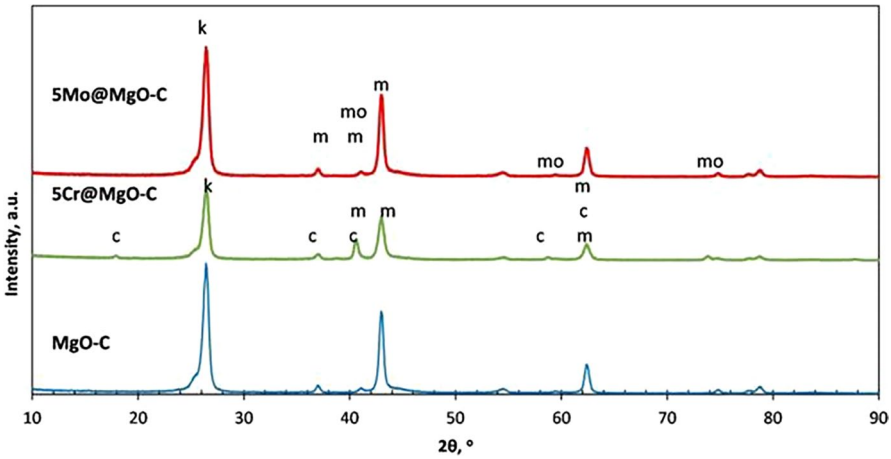


Fig. 3 XRD patterns of MgO–C-supported catalysts

relative pressures. This can be attributed to a change in the pore size of the materials since nitrogen is adsorbed in larger mesopores at higher relative pressures. Notably, the addition of active metals to the MgO support material resulted in a decrease in pore diameters due to the partial blockage of the pores (Table 1). The core–shell catalyst exhibited a surface area of 94 m^2/g with a pore diameter of 2.5 nm, while the surface area of the MgO support material measured 58 m^2/g. In the study, it was reported that the mesoporous carbon has a pore diameter of 6.2 nm and a surface area of 798 m2/g. These results confirm that encapsulating the MgO catalyst with carbon results in a large surface area and pore diameter due to enhancing the mesoporous carbon loaded into the MgO structure.

A high-resolution TEM image of a core–shell catalyst is presented in Fig. 5. This core–shell catalyst was synthesized by coating the MgO catalyst onto the mesoporous carbon catalyst. TEM analysis results demonstrated the establishment of a core–shell structure [28, 39]. Lighter particles in TEM images exhibited a MgO shell, along with lighter regions (surrounding the MgO core) indicating a mesoporous carbon core. The mesoporous carbon core was entirely encapsulated by the mesoporous MgO catalyst.

Surface morphology analysis of the catalysts was conducted using SEM. Additionally, SEM/EDX analyses were performed at different points on the catalyst surface of the monometallic catalysts to determine approximate active metal compositions. In Fig. 6, surface photographs of MgO and MgO–C-supported catalysts captured at a magnification of 5000× are provided. The analysis revealed that all synthesized materials exhibited spherical morphology with highly ordered particle sizes. Moreover, the addition of active metals did not change the structure of the support materials. The Cr or Mo contents of catalysts measured by ICP-MS and EDS analysis are reported in Table 1. The results are consistent with the nominal chemical composition of the prepared solutions, suggesting perfect dispersion of Cr and MgO particles on the surface of the support material.

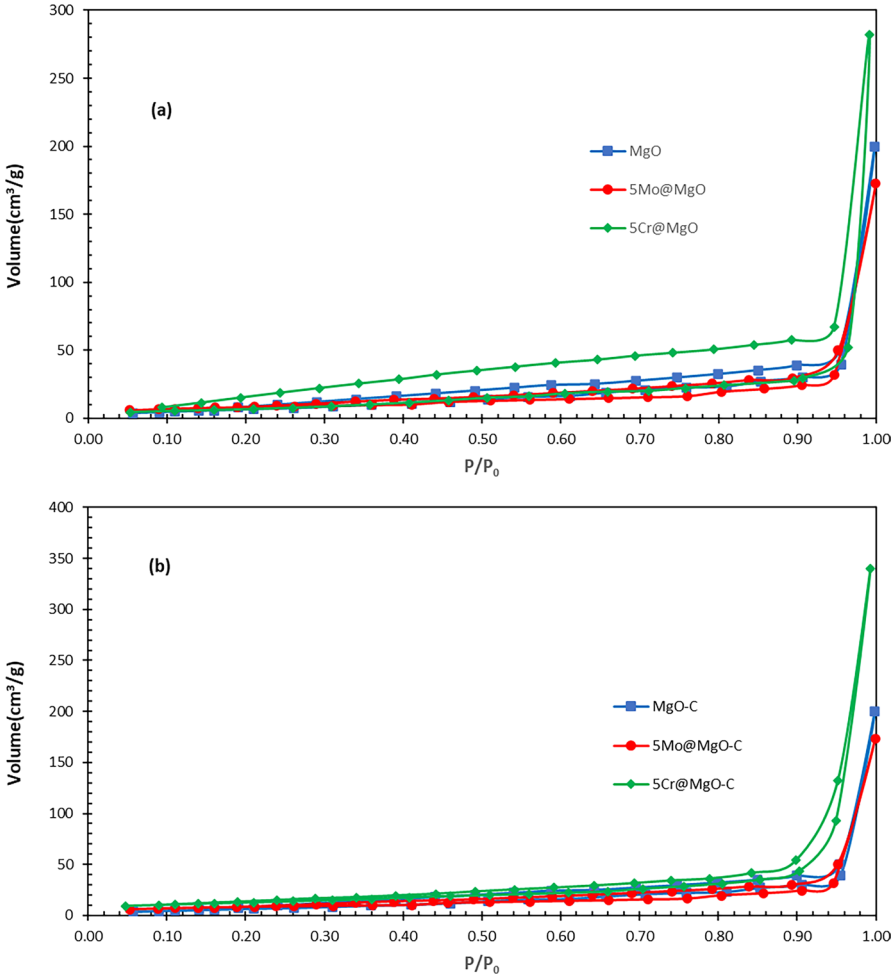


Fig. 4 N2 adsorption–desorption **a** MgO-supported catalysts; **b** MgO–C-supported catalysts

Table 1 Physical properties of the synthesized catalysts

Catalyst	Surface area, m^2/g	Average pore diameter, nm	Pore volume, cm^3/g	Active metal content, % (ICP-MS)	Active metal content, % (EDS)
MgO	58	3.9	0.069	–	–
mesoC	798	6.3	0.83	–	–
5Cr@MgO	55	3.5	0.087	4.7	5.1
5Mo@MgO	50	3.5	0.050	4.8	4.5
MgO–C	94	2.5	0.178	–	–
5Cr@MgO–C	66	2.4	0.144	4.7	5.7
5Mo@MgO–C	61	2.4	0.097	4.6	6.1

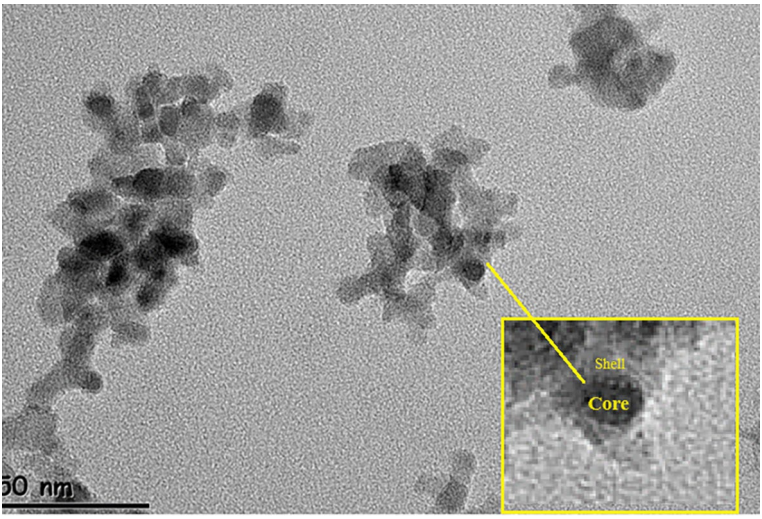


Fig. 5 TEM image of the MgO–C catalyst with a core–shell structure

Catalytic activity test results

To investigate the performance of catalysts in microwave-heated reaction systems, it is necessary for the materials to absorb microwave energy and subsequently heat up. Microwave energy absorbed by materials depends on their dielectric properties. Materials with a high dielectric constant absorb microwave energy more effectively. This absorption increases the vibration of the material's molecules, leading to an increase in temperature. When it comes to heating the catalyst bed, a catalyst with a high dielectric constant effectively absorbs microwave energy. This absorbed energy ensures rapid heating of the catalyst bed. Rapid and uniform heating helps the catalyst adapt quickly to reaction conditions and enhances reaction efficiency. Therefore, effective heating of the catalyst bed with microwaves is possible by using a catalyst with a high dielectric constant, which is crucial for accelerating the reaction process and improving efficiency. Although the MgO catalyst was capable of absorbing microwave energy, it failed to reach the required reaction temperature. Therefore, MgO-supported catalysts were mixed with a material possessing a high dielectric constant before being utilized in the microwave reaction system. Mesoporous carbon, known for its ability to absorb microwave energy and generate heat, was chosen as a suitable material. Prior to the activity tests of the MgO-supported catalysts, they were mixed with mesoporous carbon at a 1:1 weight ratio.

Preliminary experiments were conducted in the presence of mesoporous carbon. The conversion values obtained from the dehydrogenation of ethane using mesoporous carbon are presented in Fig. 7a. No conversion was observed before reaching a reaction temperature of 400 °C. At 400 °C, ethane conversion reached 11%, while at 700 °C, it reached 100%. Increasing the reaction temperature resulted in higher ethane conversion and hydrogen selectivity. This finding can be attributed

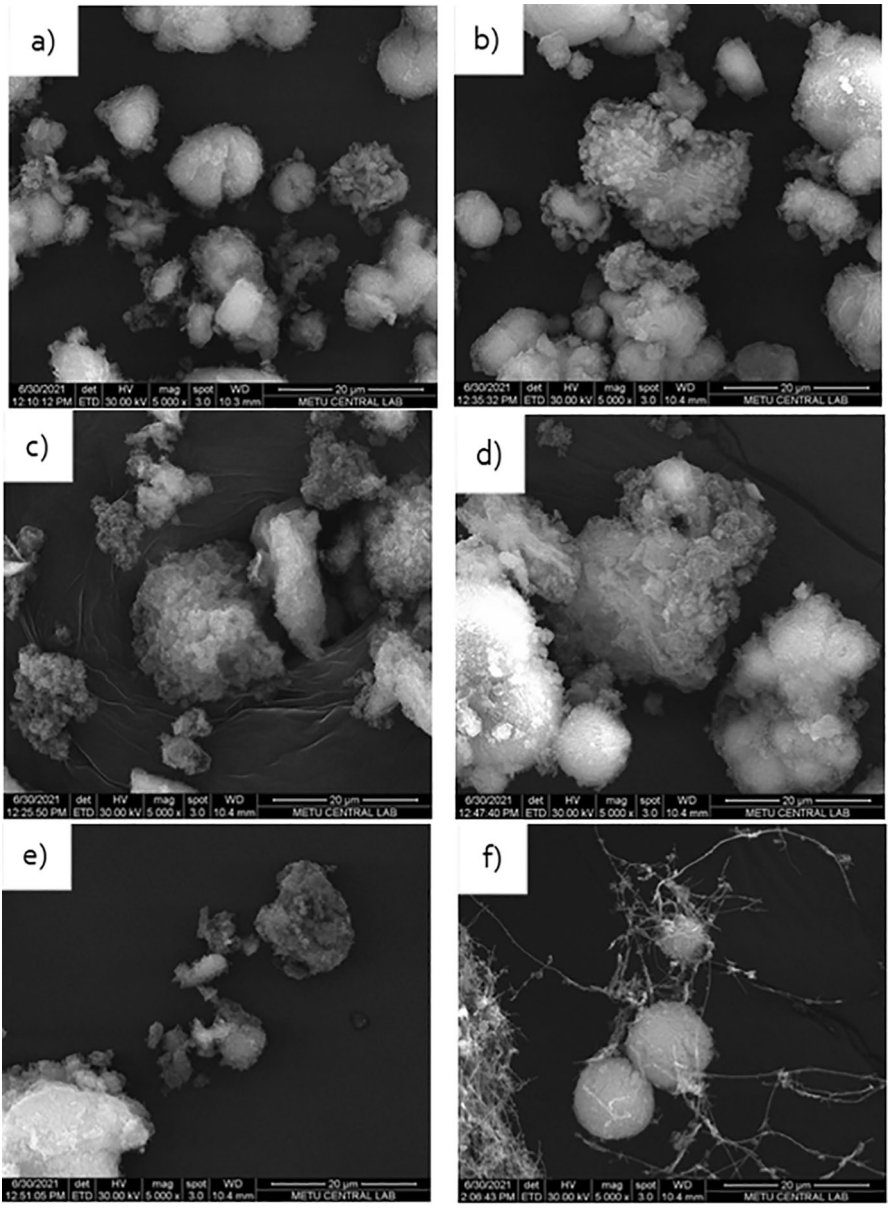


Fig. 6 SEM photographs of the synthesized catalysts: **a** MgO, **b** 5Cr@MgO, **c** 5Mo@MgO, **d** MgO–C, **e** 5Cr@MgO–C, **f** 5Mo@MgO–C

to the endothermic nature of the dehydrogenation reaction of ethane. The dehydrogenation of 1 mol of ethane yields 1 mol of hydrogen and 1 mol of ethylene. Hydrogen selectivity exceeds 1 after a reaction temperature of 550 °C (Fig. 7b). At elevated temperatures, the product distribution includes methane and acetylene in

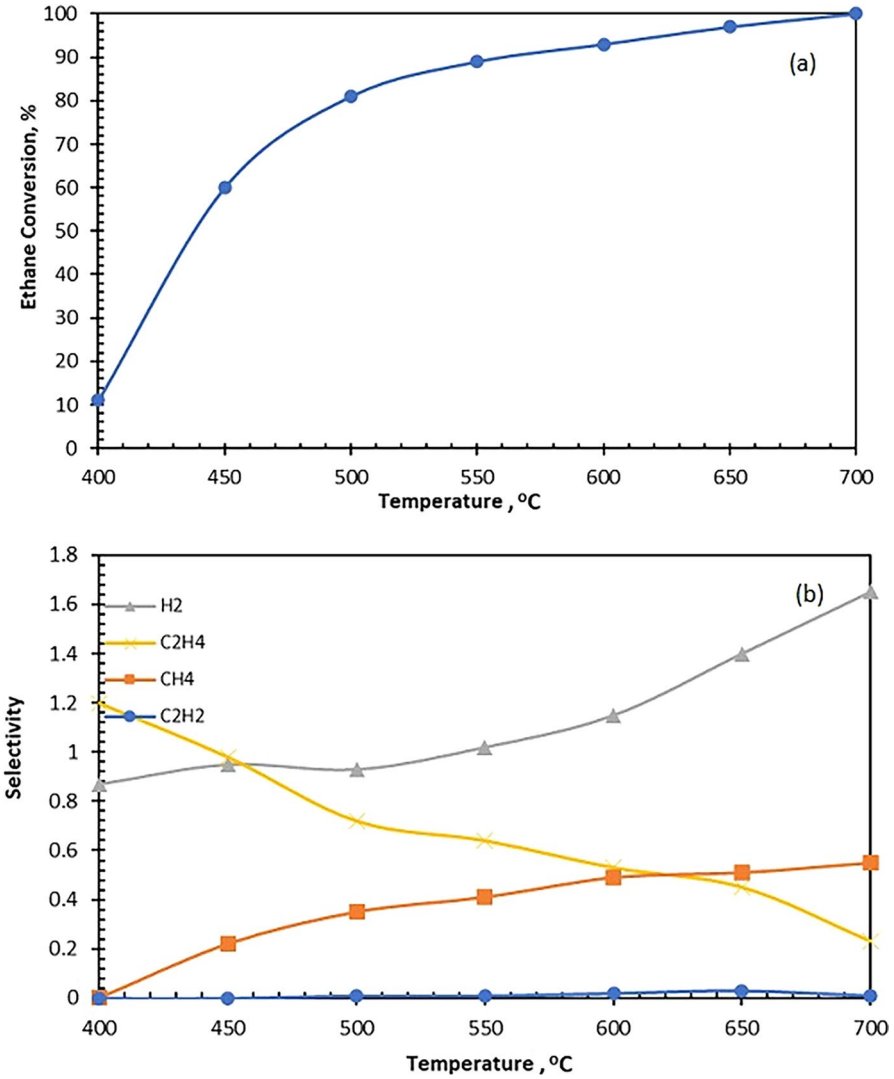


Fig. 7 Dehydrogenation reaction over mesoporous carbon (reaction conditions: 400–700 °C, 18,000 mL/h.gcat, C2H6/Ar = 1/2): **a** ethane conversion, **b** product selectivity

addition to hydrogen and ethylene. Methane is formed through the thermal decomposition reactions of ethane or ethylene (C2H6 ↔ CH4+H2+C and/or C2H4 ↔ CH4+C). Acetylene, on the other hand, is formed through the decomposition reaction of ethylene (C2H4 ↔ C2H2 + H2) [8]. These results demonstrate that higher reaction temperatures trigger side reactions.

Upon the dehydrogenation of ethane, the hydrogen/ethylene molar ratio is 1. As the reaction temperature increases, the H_2/C_2H_4 ratio also increases. The closest value to an H_2/C_2H_4 ratio of 1 was obtained at a reaction temperature of

450 °C. At this temperature, the conversion of ethane was 60%. Based on these results, the activity tests of MgO-supported catalysts were decided to be performed at a reaction temperature of 450 °C.

Activity test studies were conducted on MgO-supported catalysts containing Cr and Mo in a microwave-heated reactor system at a reaction temperature of 450 °C. MgO catalysts were mixed with mesoporous carbon with a 1:1 mass ratio. The results of the activity tests for catalysts containing Cr and Mo in the dehydrogenation of ethane are presented in Table 2. Furthermore, ethane conversions and product selectivity values of the catalysts are given in Fig. 8a–d. Comparative analysis of the ethane conversions of Cr- and Mo-containing catalysts revealed that the 5Mo@MgO catalyst exhibited superior ethane conversion performance. After 3 h of reaction time, the average ethane conversion for the 5Cr@MgO catalyst was determined to be 47%, while the 5Mo@MgO catalyst achieved an ethane conversion of 66%. Investigation of the product distributions of the catalysts revealed similar hydrogen and ethylene selectivity. In addition to ethylene and hydrogen, a small amount of methane was measured in the product distribution. The presence of methane among the products signifies the occurrence of side reactions, such as the thermal decomposition of ethane ($C2H6 \leftrightarrow CH4 + H2 + C$) and/or the thermal decomposition of ethylene ($C2H4 \leftrightarrow CH4 + C$) [8]

Among the catalysts synthesized with the incorporation of active metal, the 5Mo@MgO catalyst showed the best activity in the microwave-heated reactor system. This catalyst demonstrated the highest ethane conversion and superior hydrogen yield compared to the 5Cr@MgO catalyst. Additionally, the 5Mo@MgO catalyst demonstrated stable activity for 180 min (Fig. 8a). These results, including the high ethane conversion and hydrogen selectivity, can be attributed to the high catalytic activity of molybdenum in breaking C-H bonds. Molybdenum is known for its ability to catalyze various reactions involving carbon-hydrogen bonds [8]. Moreover, MgO support materials play crucial roles in the distribution of Mo on the catalyst surface and in providing a suitable environment for hydrogen production. The combination of the molybdenum catalyst and the MgO support is effective in achieving the desired results of high ethane conversion and hydrogen selectivity.

Table 2 Results of ethane dehydrogenation reaction in the presence of MgO and MgO–C supported catalysts in a microwave-heated reactor system (reaction conditions: 450 °C, 18,000 mL/h.gcat, C_2H_6/Ar = 1/2)

Catalyst	Conversion		Selectivity			Yield		TOF (min^{-1})
	Ethane, %	H2	C2H4	CH4	H2	C2H4	CH4	
MgO	28.7	0.94	0.98	0.03	0.27	0.28	0.01	2.14
5Cr@MgO	47.3	0.97	0.95	0.04	0.46	0.45	0.02	3.52
5Mo@MgO	65.8	0.96	0.97	0.08	0.63	0.64	0.05	4.90
MgO–C	33.5	0.93	0.90	0.03	0.31	0.3	0.01	3.22
5Cr@MgO–C	54.9	0.93	0.92	0.12	0.51	0.50	0.07	5.27
5Mo@MgO–C	72.6	0.95	0.96	0.12	0.72	0.7	0.09	6.97

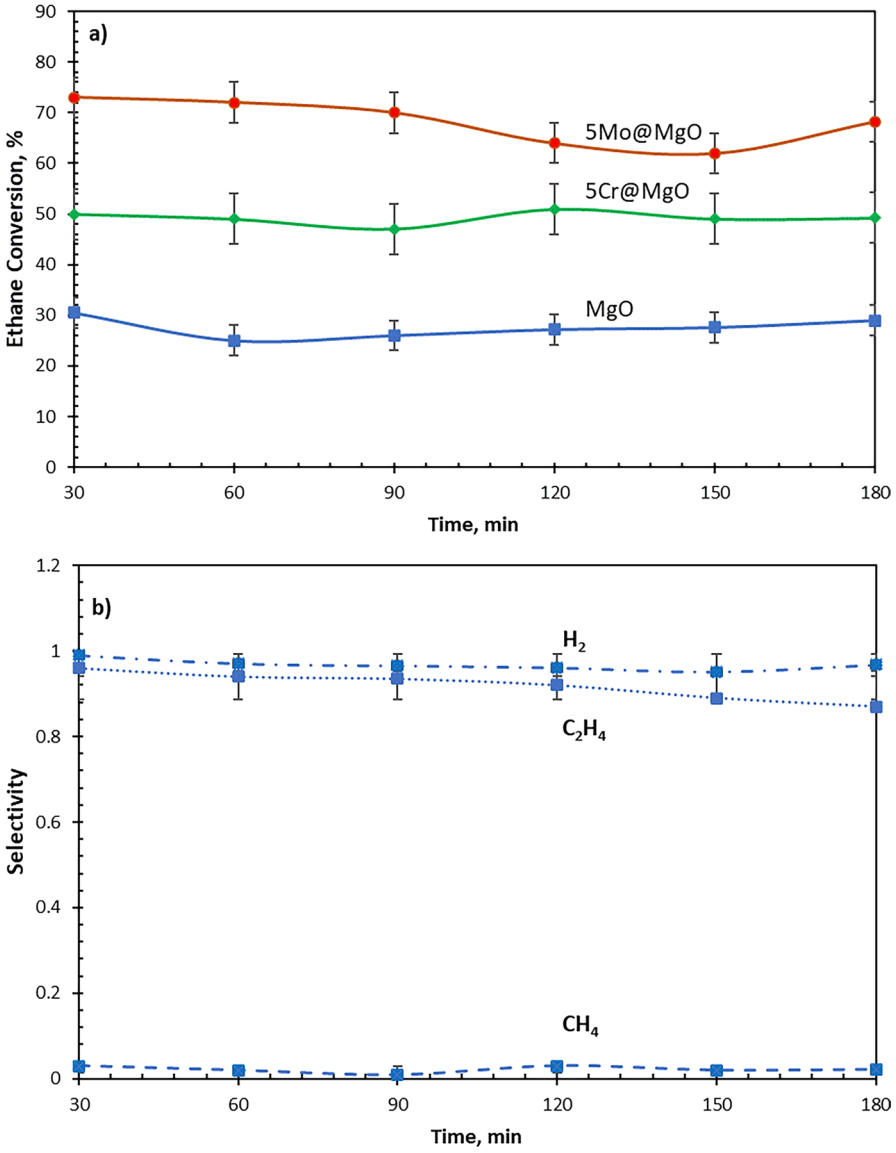


Fig. 8 **a** Time-dependent ethane conversions in the presence of MgO-supported catalysts in the dehydrogenation reaction and product selectivity of (**b**) MgO, product selectivity of (**c**) 5Cr@MgO, and **d** 5Mo@MgO catalysts (reaction conditions: 450 °C, 18,000 mL/h.gcat, C2H6/Ar = 1

The catalytic activities of MgO–C-supported catalysts were investigated in a microwave reaction system operating at a reaction temperature of 450 °C. The MgO–C support material exhibited an ethane conversion of 33.5% and hydrogen selectivity of 93%. Furthermore, the incorporation of active metals into the MgO–C catalyst led to an enhancement in ethane conversion. The 5Cr@MgO–C

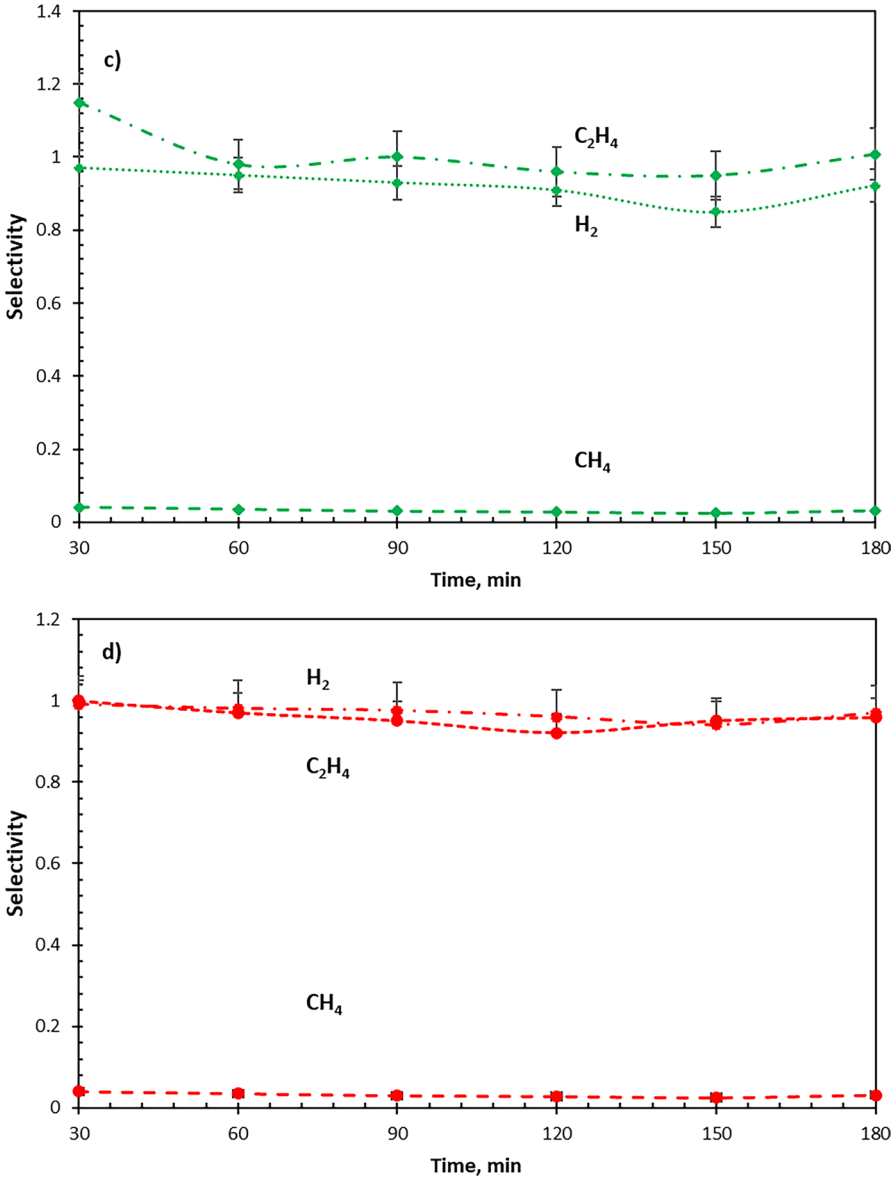


Fig. 8 (continued)

and 5Mo@MgO–C catalysts achieved conversions of 54.9% and 72.6%, respectively (Fig. 9a). A comparison between the catalytic activities of core–shell materials and physically mixed catalysts (MgO-supported materials) revealed the superior performance of the 5Mo@MgO–C catalyst. The ethane conversion of the 5Mo@MgO catalyst (Table 2) was initially measured as 65.8%, which further increased to 72.6% with the implementation of the core–shell catalyst structure.

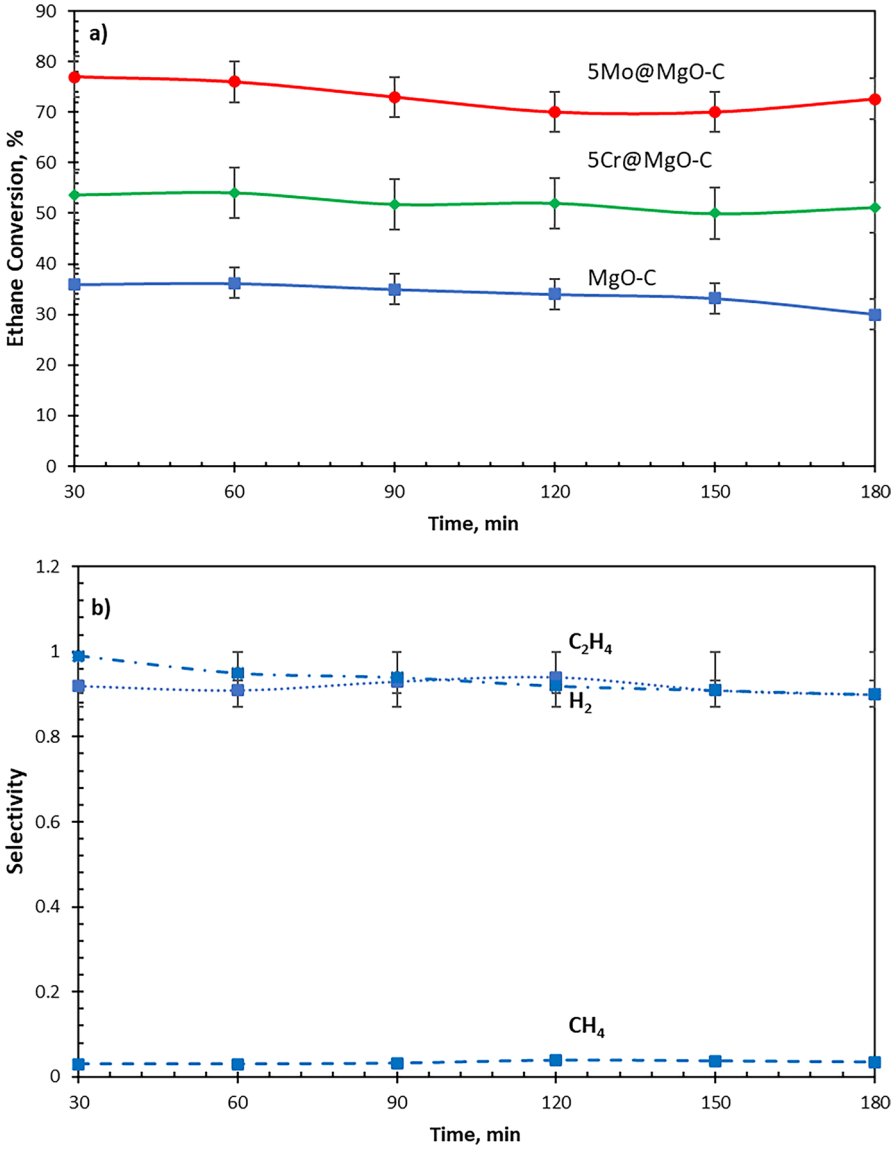
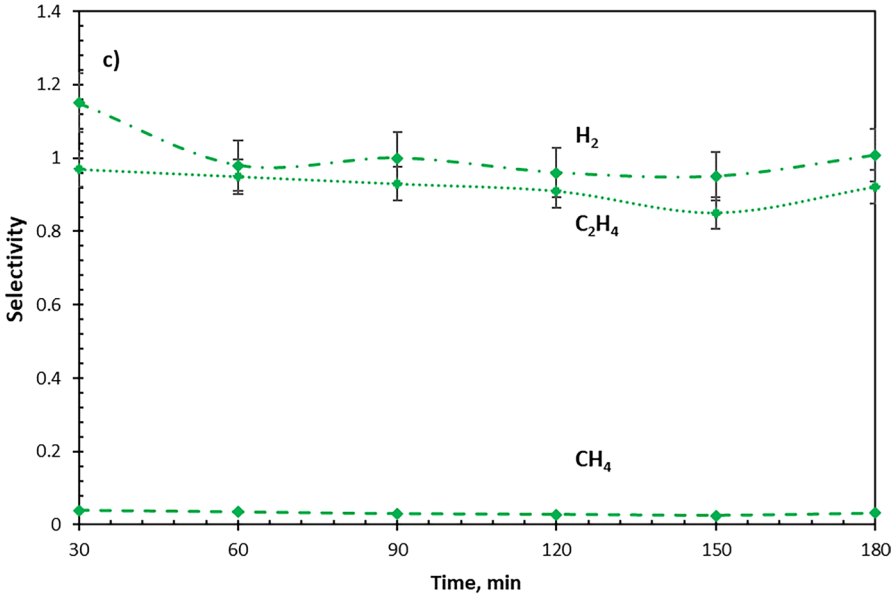


Fig. 9 **a** Time-dependent ethane conversions in the presence of MgO–C-supported catalysts in the dehydrogenation reaction and product selectivity of (**b**) MgO–C. product selectivity of (**c**) 5Cr@MgO–C, and **d** 5Mo@MgO–C catalysts (reaction conditions: 450 °C, 18,000 mL/h.gcat, C2H6/Ar = 1/2)

In the 5Mo@MgO–C catalyst, the active phase responsible for ethane dehydrogenation, represented by the 5Mo@MgO catalyst, was primarily located in the shell region. At the same time, the core section consisted of mesoporous carbon catalysts capable of absorbing microwave energy. The significantly higher catalytic activity observed in the microwave reactor system in comparison to conventional



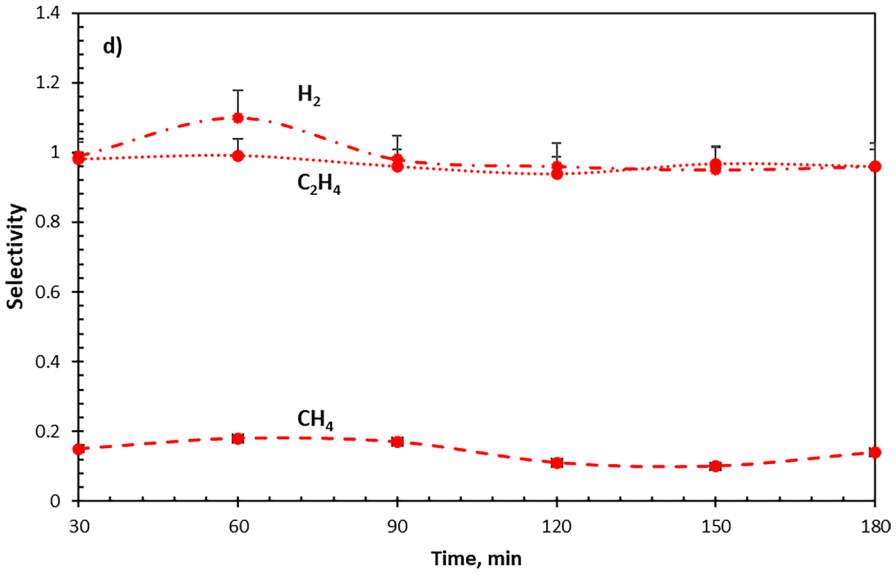


Fig. 9 (continued)

heating methods can be attributed to the formation of microplasma hotspots during the reaction [8]. These microplasmas generate considerably elevated temperatures on the catalyst surface, surpassing the measured reaction temperature. In contrast, physically mixed catalysts experience challenges in achieving a homogeneous distribution of carbon structures within the catalyst material. This non-homogeneity hinders the formation of microplasmas, which are critical for

enhancing catalytic activity. As a result, physically mixed catalysts demonstrate limited microplasma formation and, consequently, have lower levels of catalytic activity compared to core–shell catalysts. Furthermore, core–shell catalysts demonstrate a more uniform distribution of carbon throughout the catalyst material. This homogeneity promotes increased microplasma formation, leading to higher catalytic activity [8]. The presence of a well-defined core–shell structure allows for efficient interaction between the carbon content and the magnesium oxide catalyst, facilitating the generation of microplasmas. As a result, core–shell catalysts exhibit enhanced catalytic activity compared to physically mixed catalysts. In addition, it should be noted that the surface area and pore diameter of the MgO–C core–shell catalysts are higher compared to those of MgO-supported catalysts. This increase in surface area provides a larger number of active sites within the catalyst structure, which can significantly enhance product selectivity and ethane conversion. For this reason, the 5Mo@MgO–C catalyst exhibits higher catalytic activity compared to the 5Mo@MgO catalyst. The improved performance can also be attributed to the larger surface area, allowing for more efficient interactions between the catalyst and reactant molecules and thereby promoting enhanced catalytic activity and overall performance. For a more detailed examination of the catalysts' activities, turnover frequency (TOF) was calculated. Turnover number (TON) and TOF are terms used in the literature to describe catalyst activity. TON is defined as the number of molecules produced per active site before deactivation, while TOF represents the number of molecules produced at active sites during the reaction time. The formulas used for TON and TOF calculations are provided below. The calculated TOF values are presented in Table 2. Results showed that the incorporation of the active metal on the supported materials enhanced the TOF value, which provides information about the catalyst's activity. The 5Mo@MgO–C catalyst exhibits the highest ethane conversion, with its TOF value being the maximum. Furthermore, when compared to the chromium and molybdenum incorporated catalysts, molybdenum incorporated catalysts demonstrate higher values.

A literature review was conducted to compare the activity test results of the synthesized catalysts with studies reported in the literature, including those conducted in both conventional and microwave-heated reactor systems. These studies demonstrated that ethane conversion in ethane dehydrogenation using CHRS is less than 25% [20, 39, 40]. Robinson et al. explored the catalytic activity of ZSM-5 supported Mo and Fe catalysts in both microwave and conventional heating systems. They achieved an 80% ethane conversion at 660 °C in CHRS and 375 °C in MWHRS [25]. Additionally, Eryıldırım et al. found that the 5Cr@SBA-15 catalyst exhibited negligible catalytic activity below 650 °C in CHRS, but 40.5% ethane conversion was observed at 400 °C in MWHRS. The ethane conversion values achieved at 450 °C in MWHRS were similar to those at 650 °C in CHRS [8]. In the MWHRS system, Eryıldırım et al. reported a maximum conversion of 49.9% with the 5Cr@SBA-15 catalyst. However, the 5Mo@MgO–C catalyst demonstrated superior activity, achieving a maximum ethane conversion of 72.6% in this study. This result could be attributed to the core–shell structure of the 5Mo@MgO–C catalyst, which leads to a homogeneous distribution of the active sites. Therefore, the 5Mo@MgO–C catalyst

shows promising potential for ethane dehydrogenation applications. Furthermore, all studies in the literature consistently report that MWHRS exhibits enhanced selectivity for hydrogen and ethylene. [8, 20, 25, 39, 40].

Effect of reaction temperature

At 350 °C, the ethane conversion using the 5Mo@MgO–C catalyst achieved a conversion of 40%. As the reaction temperature increased, ethane conversion also increased. At 500 °C, the ethane conversion with the 5Mo@MgO–C catalyst reached 81%, and at 650 °C, it further increased to 98%. Since ethane dehydrogenation is an endothermic reaction, the conversion tends to rise with higher reaction temperatures. However, the results indicated that as the reaction temperature increased, selectivity to ethylene decreased. At lower temperatures, the primary reaction pathway is the dehydrogenation of ethane (C_2H_6) to produce ethylene (C_2H_4) and hydrogen (H_2), as shown in Eq. (1). However, at these lower temperatures, the side reactions described by Eq. (15) become more significant.

$$C_2H_6 \rightarrow C_2H_4 + H_2 \quad \Delta H^{\circ}_{298} = 136.4\,\mathrm{kJ/mol} \tag{1}$$

$$C_2H_6 \leftrightarrow CH_4 + 1/2\,C_2H_4 \quad \Delta H^{\circ}_{298} = 35,6\,\mathrm{kJ/mol} \tag{15}$$

Reaction conditions (lowered reaction temperature) contributed to increased ethylene production. Specifically, ethane was converted to ethylene through the decomposition reaction, so lower temperatures favored ethylene production both kinetically and thermodynamically, making ethylene the important side product. Moreover, the enthalpy of the ethane dehydration reaction is higher than that of the decomposition reaction (Eq. 15), indicating that it requires more energy. Thus, as the temperature increases, the rate of the main dehydrogenation reaction (Eq. 1) also increases. However, the rate of the side reactions (Eq. 13) increases even more rapidly. This results in a decrease in ethylene selectivity and a corresponding increase in selectivity towards methane (Fig. 10).

As the reaction temperature increases, hydrogen selectivity rises while ethylene selectivity declines. The decrease in ethylene selectivity is attributed to methane formation from both ethane and ethylene. Additionally, the C_2H_4/H_2 ratio was 1 at 450 °C, indicating that only the main reaction occurred at that temperature. With an increase in temperature, the C_2H_4/H_2 ratio fell below 1. Surpassing hydrogen selectivity at elevated temperatures decreases the ethylene-to-hydrogen ratio, explained by the dominance of side reactions. Acetylene is formed in trace amounts at higher reaction temperatures. The presence of acetylene confirms the occurrence of side reactions. Therefore, the reaction temperature of 450 °C can be considered the most suitable for ethane dehydrogenation in this microwave-heated reactor system (Fig. 11).

$$C_2H_6 \leftrightarrow CH_4 + H_2 + C \quad \Delta H^{\circ}_{298} = 9,3\,\mathrm{kJ/mol} \tag{3}$$

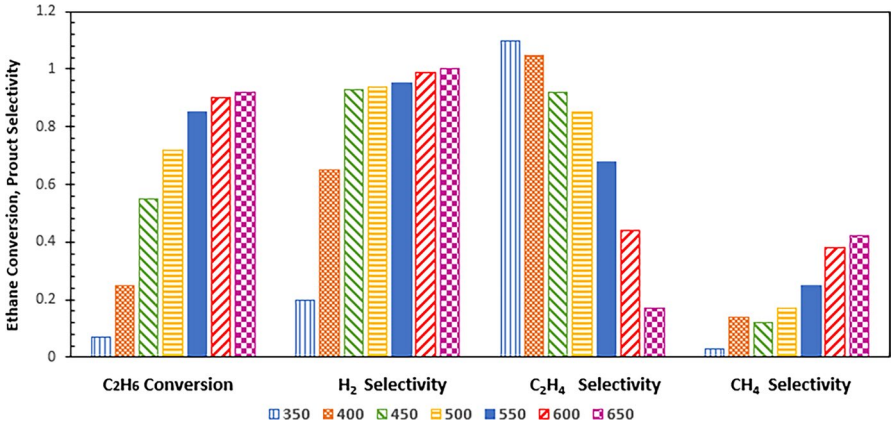


Fig. 10 Activity Test Results of 5Cr@MgO–C Catalyst at Different Reaction Temperatures (Reaction Conditions: 350–650℃, 18,000 ml/h.gcat, C_2H_6/Ar = 1/2)

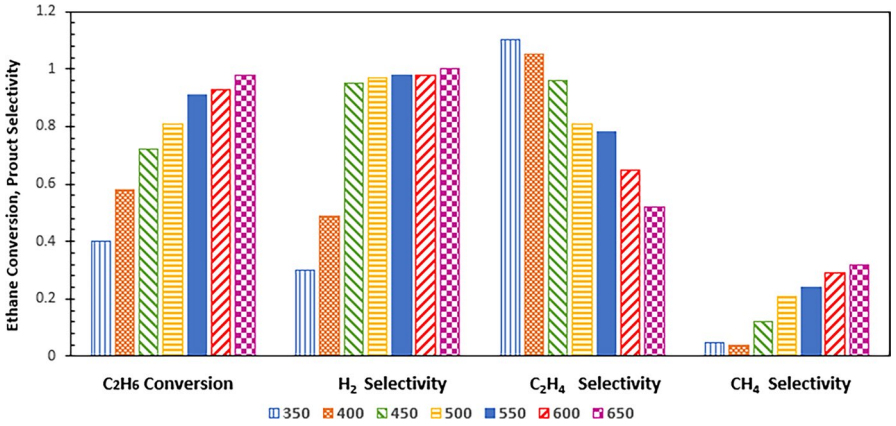


Fig. 11 Activity Test Results of 5Mo@MgO–C Catalyst at Different Reaction Temperatures (Reaction Conditions: 350–650℃, 18,000 ml/h.gcat, C_2H_6/Ar = 1/2)

$$C_2H_6 \leftrightarrow 3H_2 + 2C \quad \Delta H^{\circ}_{298} = 83,8 \text{ kJ/mol} \tag{6}$$

$$C_2H_4 \leftrightarrow C_2H_2 + H_2 \quad \Delta H^{\circ}_{298} = 175 \text{ kJ/mol} \tag{8}$$

Coke analysis of the spent catalysts

The thermogravimetric analysis (TGA) profiles of the MgO–C and 5Mo@MgO–C catalysts after 3-h activity tests at 450 °C are presented in Fig. 12. The two main reactions that cause carbon formation in the activity studies of catalysts are the Boudouard ($2CO \leftrightarrow C + CO_2$) and methane decomposition ($CH_4 \leftrightarrow C + 2H_2$) reactions

[5]. These reactions causing coke formation could lead to deactivation of the catalyst by clogging the active sites. The TGA results show that weight loss up to 200 °C is attributed to the evaporation of water from the catalyst structure. Weight losses observed from 400 °C onward are due to the removal of carbon deposits that had built up on the catalysts during the tests. For the MgO–C catalyst, a 15% weight loss was observed, while the 5Cr@MgO–C catalyst had only an 11% weight loss. The addition of active metal reduced coke formation. When examining the DTA results in Fig. 12, peaks originating from carbon were observed in the range of 300–500 °C. It is known in the literature that carbon peaks seen at temperatures below 500 °C indicate amorphous carbon and filament-type carbon disappears in the range of 500–750 °C [28]. As a result of the activity test studies with DTA analysis, it was determined that amorphous-type carbons were formed on the surface of the catalysts.

Conclusion

In this study, innovative catalysts for ethane dehydrogenation were successfully synthesized by incorporating chromium and molybdenum into MgO- and MgO–C-supported catalysts. The catalysts were characterized using various analytical techniques, and their catalytic activities were evaluated in a microwave-heated reactor system. Among the synthesized catalysts, Mo- incorporated catalysts exhibited the highest catalytic activity thanks to their advanced C-H bond-breaking capacity. Moreover, the highest ethane conversion was obtained in the presence of the 5Mo@MgO–C catalyst. In the microwave heating reaction system (MWHRS), heat is delivered directly to the catalyst, forming micro-plasmas (hot spots) within the catalyst that boosts catalyst activity. These microplasmas produce better ethane conversion than the conventionally heated reaction system (CHRS). Furthermore, the microwave heating system achieves more significant energy efficiency by

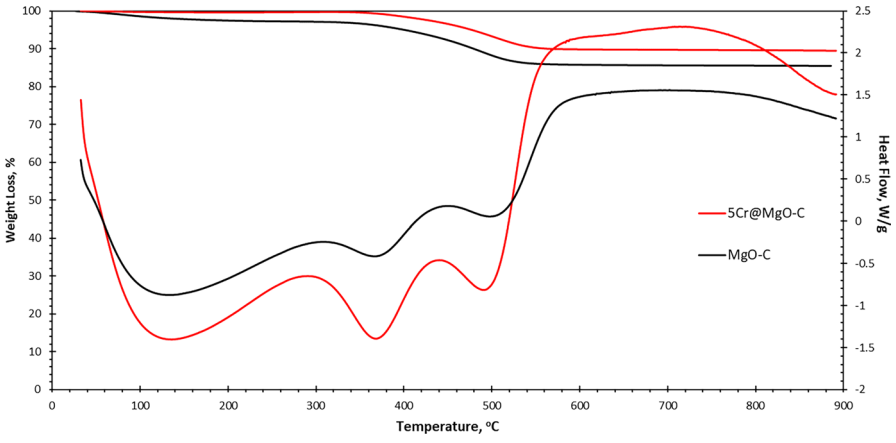


Fig. 12 TGA and DTA results of MgO–C and 5Cr@MgO–C catalysts

minimizing energy losses from heating the furnace wall and cavity, unlike CHRS. To achieve similar conversion values in both systems, MWHRS requires 0.04 kW of electricity for the activity test at 450 °C, while CHRS uses 0.8 kW at 650 °C. The results demonstrate that heating with microwave radiation is 20 times more energy-efficient than standard electric heating systems. MgO-encapsulated carbon-core catalysts with Mo and Cr exhibit high activity and selectivity for ethane dehydrogenation, making them promising for industrial-scale applications. This study highlights the significant advantages of microwave-heated reaction systems, including reduced energy consumption and increased efficiency, which make hydrogen production more economical. Moreover, core–shell catalysts suggest potential advancements in activity, addressing challenges faced by physical mixing catalysts. This study provides innovative approaches and detailed insights that could pave the way for developing new catalysts and reaction systems tailored for ethane dehydration reactions, enhancing their industrial applicability and efficiency. However, challenges such as precise optimization and control of microwave-heated reaction systems should be addressed for successful industrial application. Moreover, the primary challenge associated with core–shell catalysts lies in the high cost of the mesoporous carbon catalyst. Additionally, the presence of carbon in the catalyst structure can pose difficulties during regeneration processes. Regeneration of carbon-containing catalysts in an air environment can lead to structural impairments; therefore, they should be regenerated under an inert gas atmosphere (N_2, etc.) to maintain their integrity and functionality. However, when all the pros and cons related to this catalyst and microwave system are compared, it is clear that the industrial potential of the study is significantly high.

Supplementary Information The online version contains supplementary material available at https://doi.org/10.1007/s11164-024-05309-2.

Acknowledgements The authors gratefully acknowledge the financial support provided by the Scientific and Technological Research Council of Turkey (TUBITAK 121M963) and the Gazi University Research Fund (BAP-06/2018-13). Thanks to Prof. Dr. Timur Doğu, Prof. Dr. Nuray Oktar, and Saleh Ahmat Ibrahim for their support. Thanks to the central laboratory of METU for the characterization results of the synthesized catalysts.

Author contributions Birce Karaman: Investigation, Methodology, Validation, Performing of experimental testsEmine Ekinci:Supervision, Investigation, Conceptualization, Validation, Performing of experimental tests

Funding Open access funding provided by the Scientific and Technological Research Council of Türkiye (TÜBİTAK).

Declarations

Competing interests The authors declare no competing interests.

Open Access This article is licensed under a Creative Commons Attribution 4.0 International License, which permits use, sharing, adaptation, distribution and reproduction in any medium or format, as long as you give appropriate credit to the original author(s) and the source, provide a link to the Creative Commons licence, and indicate if changes were made. The images or other third party material in this article are included in the article's Creative Commons licence, unless indicated otherwise in a credit line to the material. If material is not included in the article's Creative Commons licence and your intended

use is not permitted by statutory regulation or exceeds the permitted use, you will need to obtain permission directly from the copyright holder. To view a copy of this licence, visit http://creativecommons.org/licenses/by/4.0/.

References

1. Y.A. Al-Baqmaa, A.S. Al-Fatesh, A.A. Ibrahim, A.A. Bagabas, F.S. Almubadde, A.I. Alromaeh, A.H. Fakeeha, Res. Chem. Intermed. **49**, 5015–5028 (2023)
2. M.S. Yancheshmeh, S.S. Haghighi, M.R. Gholipour, O. Dehghani, M.R. Rahimpour, S. Raeissi, Chem. Eng. J. **215**, 550–560 (2013)
3. K. Fujimoto, K. Tomishige, O. Yamazaki, Y. Chen, X.H. Li, Res. Chem. Intermed. **24**, 259 (1998)
4. S.A. Ibrahim, E.K. Ekinci, B.P. Karaman, N. Oktar, Int. J. Hydrogen Energy **46**, 38281–38298 (2021)
5. M.Y. Dogan, H. Arbag, H.M. Tasdemir, N. Yasyerli, S. Yasyerli, Int. J. Hydrogen Energy **48**, 23013–23030 (2023)
6. T.X. Nguyen-Thi, P.Q.P. Nguyen, V.D. Tran, Ü. Agbulut, L.H. Nguyen, D. Balasubramanian, Int. J. Hydrogen Energy **54**, 127–160 (2024)
7. S. Kim, J. Song, H. Lim, Korean J. Chem. Eng. **35**, 1509–1516 (2018)
8. B. Eryildirim, H. Arbag, N. Oktar, G. Dogu, Int. J. Hydrogen Energy **7**, 5296–5310 (2021)
9. J.M. Bermúdez, D. Beneroso, N. Rey-Raap, A. Arenillas, J.A. Menéndez, Chem. Eng. Process Process Intensif **95**, 1 (2015)
10. A. Domínguez, B. Fidalgo, Y. Fernández, J.J. Pis, J.A. Menéndez, Int. J. Hydrogen Energy **32**(18), 4792–4799 (2007)
11. T. Durka, G.D. Stefanidis, T. Van Gerven, A.I. Stankiewicz, Int. J. Hydrogen Energy **36**, 12843–12852 (2011)
12. K.K. Rana, Rana. S. Oalib. **1**, 1–20 (2014)
13. R.C. Seyfeli, D. Varisli, Int. J. Hydrogen Energy **45**, 34867–34878 (2020)
14. S. Gündüz, T. Dogu, Appl. Catal. B **168**, 497–508 (2015). https://doi.org/10.1016/j.apcatb.2015.01.006
15. R.C. Seyfeli, D. Varisli, Int. J. Hydrogen Energy **34**, 15175–15188 (2022)
16. D. Varisli, C. Korkusuz, T. Dogu, Appl. Catal. B **201**, 370–380 (2017)
17. M. Guler, C. Korkusuz, D. Varisli, Int. J. Chem. Reactor Eng. **17**, 20180162 (2019)
18. X. Ren, M.S. Ghazani, H. Zhu, W. Ao, H. Zhang, E. Moreside, X. Bi, Appl. Energy **3**, 118970 (2022)
19. M. Guler, T. Dogu, D. Varisli, Appl. Catal. B **219**, 173–182 (2017)
20. H. Yang, L. Xu, D. Ji, Q. Wang, L. Lin, React. Kinet. Catal. Lett. **76**, 151–159 (2002)
21. Y. Wang, C. Tang, K. Ma, X. Li, Surf. Interfaces **42**, 103524 (2023)
22. S.Y. Chin, Y.H. Chin, M.D. Amiridis, Appl. Catal. A **300**, 8–13 (2006)
23. Z. Jia, C. Tang, K. Ma, X. Li, Chem. Commun. **59**, 9235–9238 (2023)
24. A.K. Rovik, S.K. Klitgaard, S. Dahl, C.H. Christensen, I. Chorkendorff, Appl. Catal. A Gen. **358**, 269–278 (2009)
25. U. Olsbye, A. Virnovskaia, Ø. Prytz, S.J. Tinnemans, B.M. Weckhuysen, Catal. Lett. **103**, 143–148 (2005)
26. S. Lillehaug, K.J. Borve, M. Sierka, J. Sauer, J. Phys. Org. Chem. **17**, 990 (2004)
27. X. Yang, Y. Weng, M. Li, B. Sun, Y. Li, Y. Wang, Energy Fuels **30**, 2198–2203 (2016)
28. H. Arbag, Int. J. Hydrogen Energy **43**, 6561–6574 (2018)
29. F. Bastan, M. Kazemeini, A. Larimi, H. Maleki, Int. J. Hydrogen Energy **43**, 614–621 (2018)
30. B.P. Karaman, N. Oktar, G. Doğu, T. Dogu, Catalysts **12**, 1102 (2022). https://doi.org/10.3390/catal12101102
31. C. Bao, A. Serrano-Lotina, M. Niu, R. Portela, Y. Li, K.H. Lim, Q. Wang, Chem. Eng. J. **466**, 1385–8947 (2023)
32. K.W. Shah, G.F. Huseien, H.W. Kua, Micro. **1**, 55–85 (2021)
33. B.M. Al-Swai, N.B. Osman, B. Abdullah, AIP Conf. Proc. 1891 (2017)
34. J. Zhou, N.S. Xu, S.Z. Deng, J. Chen, J.C. She, Z.L. Wang, Adv. Mater. **15**, 1835–1840 (2003)
35. M.C. Ozcan, B.P. Karaman, N. Oktar, T. Dogu, Fuel **330**, 125607 (2022)
36. P. Degirmencioglu, H. Arbag, Arabian J. Sci. Eng. (2023)
37. B.P. Karaman, N. Cakiryilmaz, H. Arbag, N. Oktar, G. Dogu, T. Dogu, Int. J. Hydrogen Energy **42**, 26257–26269 (2017)
38. D.K. Kim, C.Y. Cha, W.T. Lee, J.H. Kim, J. Ind. Eng. Chem. **7**, 363–374 (2001). https://doi.org/10.1007/s13203-013-0024-z

39. F. Akti, J. Poly. Environ. **29**, 2236–2247 (2021)
40. A. Tsyganok, P.J. Harlick, A. Sayari, Catal. Commun. **8**, 850–854 (2007)
41. B. Robinson, A. Caiola, X. Bai, V. Abdelsayed, D. Shekhawat, J. Hu, Catal. Today **356**, 3–10 (2020)

Publisher's Note Springer Nature remains neutral with regard to jurisdictional claims in published maps and institutional affiliations.